Brazilian Journal of Geophysics, **42** (2024), 3, 1–21
Brazilian Geophysical Society
ISSN 2764-8044
DOI 10.22564/brjg.v42i3.2325

BUILDING A 3D MODEL IN THE TIME-DOMAIN OF THE VERTICAL-VERTICAL CONTROLLED-SOURCE ELECTROMAGNETIC METHOD

Danusa Mayara Souza, Marcos Welby Correa Silva and Victor Cezar Tocantins

Universidade Federal do Pará - UFPA, Belém, PA, Brazil

*Corresponding author: welbysilva@gmail.com

ABSTRACT. The exploratory activity involves several uncontrollable factors, such as the presence or absence of oil and the quality of the extracted product. To minimize uncertainties and ambiguities encountered during oil and gas prospecting, controlled-source electromagnetic methods in the marine environment have gained prominence owing to technological and operational innovations. Studies have shown that the Marine Controlled-Source Electromagnetic (MCSEM) method is suitable and sustainable for directly indicating hydrocarbons. In order to optimize MCSEM further, the source-receiver configuration as well as its reading mode were changed, creating the Vertical-Vertical Controlled-Source Electromagnetic (VVCSEM) method. We tested the source and receiver arrangements, modeled in a multiphysics modeler the VVCSEM method, and analyzed the promise which was developed to have a higher vertical resolution and promoting a clear distinction between conductive and resistive bodies. In this manuscript, we suggest constructing the modeling of the VVCSEM in steps. There are two steps for the modeling: the source response (switch-on) in the stationary regime and recording of the electromagnetic field interaction by the receivers in the transient regime. As reported previously in the benchmark literature, the VVCSEM effectively detected the suggested resistive anomalies.

Keywords: transient electromagnetic method; electromagnetic modeling; vertical electric dipole; hydrocarbon reservoir monitoring; marine geophysical methods.

INTRODUCTION

Supported by a substantial body of research for direct indication of hydrocarbons (Sainson, 2017), the marine controlled-source electromagnetic (MCSEM) method was changed in its acquisition configuration to improve vertical resolution and avoid direct waves and airwaves (Flekkøy et al., 2009; Frafjord et al., 2014). In addition to instrumental changes, the method was named vertical-vertical controlled-source electromagnetic (VVCSEM). It was patented under the names transient electromagnetic prospecting with vertical electric lines (TEMP-VEL) and transient electromagnetic prospecting with adjusted electric lines (TEMP-AEL) for use in shallower waters (Helwig et al., 2016).

The VVCSEM approach is essentially an MCSEM method that differs from seabed logging (SBL), a method that has become synonymous with electromagnetic source-controlled methodologies, by the source-receiver loop configurations and use of the time-domain – instead of the frequency domain – as an acquisition mode. It is mostly used for monitoring hydrocarbon reservoirs and making a clearer distinction between conductive and resistive bodies using near-field imaging and performing punctual time-lapse.

Although VVCSEM surveys are less expensive than seismic surveys and cause a lower environmental impact, they also have a considerable operating cost; in these cases, numerical modeling is an excellent tool for realistic simulations. The use of computer models is crucial to analyzing the behavior of various geophysical methodologies. Thus, the motivation of this study was to analyze the response of the VVCSEM method in a canonical geological model and verify the electromagnetic field behav-

ior in different configurations, e.g., variations in water layer thickness, reservoir layer thickness, Tx tilt ($-10°, +10°, -20°and + 20°$), and presalt and post-salt reservoir analyses. Furthermore, this manuscript serves as a tutorial for young scientists, students, as well as professionals who want to analyze VVCSEM in different geological models using modeling.

In practice, the challenge of transient modeling methods is to simulate the fading response of the electromagnetic field and its interactions with the subsurface environment in the face of contrasting physical properties. Computationally, two collection options are accepted: the first is to read the data and measure the level of disturbance of the geological features by the source. The second is to read the data taken after the source is turned-off. In the case of the VVCSEM, the second option is the most reliable. The VVCSEM takes measurements of subsurface properties over time intervals. Transient situations are complicated to model because readings and data collection are made at the same time while the source is inoperative (switched off) and the geological environment is still excited by the stimulus from the recently turned-off source.

In this manuscript, we suggest constructing the modeling of the VVCSEM in steps. There are two steps for the modeling: the source response (switch-on) in the stationary regime and the recording of the electromagnetic field interaction by the receivers in the transient regime. The validation of the multi-physics VVCSEM response was based on the benchmark articles (Holten et al., 2009; Helwig et al., 2019), as well as simulations using Python. See Souza et al. (2022), which provide the VVCSEM Python codes in Zenodo and GitHub repositories.

METHODS

The VVCSEM and the Modeling Challenges

Similarly to the MCSEM method, the VVCSEM performs subsurface electromagnetic field measurements in a marine environment. The acquisition system is formed by a vertically oriented source (Tx) and a receiver (Rx), transported by a ship and arranged for data collection by cranes. According to Helwig et al. (2016), for subsurface resistivity measurements in an offshore acquisition, a vertical dipole source and a vertical receiver have various benefits. However, to fully utilize the capabilities of this methodology, the source-receiver assembly must meet stringent requirements in terms of noise levels and verticality.

The transmitter has particular features to avoid one of the biggest problems affecting MCSEM data, namely the airwaves; therefore, a time function is employed in the VVCSEM to avoid them on the source. Mathematically, the turned-off source is a scaled version of $H(-t)$, for which $H(t)$ is the Heaviside step function. Before the source is switched off, the electric field has an initial value $E(0)$ determined by an 'everlasting' current (in principle). However, when $t = 0$, when the current of the source is turned-off, the electric field magnitude immediately jumps to a lower value owing to attenuation on the ground. This situation is followed by a drop to zero, and the magnitude of the jump and the exact shape of the decay curve depend on the electric conductivity structure below the source and the receiver.

The source function is a scaled version of the Heaviside function H(t). The electric field of the receiver (E) is initially zero because of the source. When the source current is turned on, there is an immediate jump in the field, followed by further increases in magnitude, tending to the final value E(0). The shut-down response E- and the activation response E+ are related so that

$$E(t) = -E(t) + E(0), \tag{1}$$

which is the switch-on response, represented by the switch-off response, plus a constant known from the initial switch-off value. The constant can be difficult to determine if the data are noisy. One solution is to use a long-period square wave as a source time function.

In addition to the pulse generator, Tx is also composed of a vertical electric dipole (VED) (5000 Ampère) consisting of two steel electrodes (2500 A, each one) connected by a long copper cable, with the first electrode 50 meters below the water surface and the second on the seabed. An A-frame electrode launcher/retrieval crane positions the electrodes carefully, minimizing the bending of the transmitter cable.

The tiny amplitude of the signal poses a challenge when measuring the vertical component of the electromagnetic field rather than the horizontal one. At end times, the horizontal response of a horizontal dipole is 2-3 orders of magnitude more substantial than the vertical response of a vertical dipole. Therefore, the tilt angles of both the transmitter and the receiver need to be kept as small as possible, a difficulty that prompted the development of a tripod antenna in which the action of gravity establishes verticality. Tilt effects can also be controlled by the dependency of the data measured on the transmitter and the positions of the receiver. The receivers are composed of nonferrous material in each tripod antenna. A top electrode unit, a bottom electronic unit (batteries, data storage and recording unit) and a sand ballast (which serves as weight for the descent of the Rx) are decoupled at the end of data acquisition. A system called "buoy-bell" promotes a better vertical alignment through the balance between the weight of the "bell" (a heavy structure whose shape resembles a bell as it is concave downwards) and the buoyancy force of the "buoy" (a spherical structure that resembles a sea buoy inside the bell).

The receivers are placed at the bottom of the sea, and field information is retrieved after they return to the ship or via cables connected to the receiver base. An ROV (remotely operated vehicle) spreads and connects/disconnects the crane hooks and the optical fiber (which receives data in real time). This manuscript represents the tripod antenna as a point element since it demonstrated the same response as the tripod but a lower computational expense.

The Rx recorded electric field information, in addition to data on navigation, source and status. More detailed instrumental information can be found in Barsukov et al. (2007, 2008) and Kjerstad (2010), which are the patents for TEMP-VEL, TEMP-AEL and the receivers, respectively.

The data acquisition is made in the time domain, where both the source and the receivers remain static. The electromagnetic field information is read by the receiver during periods of inactivity of the source. The source is turned on when the receivers are off; thus, the measurements are not interfered by direct waves and airwaves, which are inherent drawbacks of SBL acquisitions. Figure 1 shows a comparative illustration of the MCSEM and VVCSEM methods and further explains them. In the VVCSEM data acquisition scheme (on the right), a stationary submerged source (a VED) oscillates between on and off periods. Receivers pick up the pulse and scatter it on the ocean floor during source inactivity.

For analysis of the collected data, a comparison is made between the responses in environments (or models) with no hydrocarbons ($NoHC$) $E_0(t)$ and the responses in environments with hydrocarbons (HC) $E_{HC}(t)$; thus, the altered vertical field is:

$$E_A = E_0(t) - E_{HC}(t), \tag{2}$$

and the contrast is

$$S = 1 - \frac{E_{HC}(t)}{E_0(t)}, \tag{3}$$

The contrast is as important as the anomaly itself. The discrepancy is primarily determined by the transverse resistivity of the overburden, which is equal to the thickness multiplied by the resistivity, compared to the transverse resistivity of the reservoir. The difference between NoHC responses and a 1D HC reservoir is relatively continuous over a radius of approximately 2000 m if the reservoir is deeper than 1000 m. At extremely short offsets (less than 300 m), small Rx movements generate uncertainty and induced polarization (IP) effects. In some cases, they can dominate the measurements, although at more significant offsets (more than 1000 m), there is increased contribution of three-dimensional and tilt effects. The ideal offset between these limits of the vertical-vertical (Tx and Rx) arrangement is usually 250 m - 1500 m. The characteristic short offset causes the imaging to be near the zone (focused), and the $Tx - Rx$ configuration causes only the transverse magnetic mode of the electromagnetic field to propagate.

The Physics of the Method

Starting from Maxwell's time-domain equations in a half-space to better elucidate the VVCSEM methods, we have the following equations:

$$\nabla \times e - \mu_0 \frac{\partial h}{\partial t} = 0, \tag{4}$$

and

$$\nabla \times h - \varepsilon_0 \frac{\partial e}{\partial t} = 0, \tag{5}$$

where e and h are the electric field (V/m) and the magnetic field (A/m), respectively. $\mu_0$is the magnetic permeability ($4\pi \times 10^{-7}$) and ε_0 is the electric permittivity (8.85×10^{-12}). For the material world, there are the Faraday and Ampère laws:

$$\nabla \times e + \frac{\partial b}{\partial t} = -j^m, \tag{6}$$

and

$$-\nabla \times h + \frac{\partial d}{\partial t} + j = -j^e, \tag{7}$$

where b and d are the magnetic induction (Wb/m^2) and the dielectric displacement (C/m^2), and j^e and j^m are the external electric and magnetic current density volumes, respectively.

The method starts by transforming equations (6) and (7) to the frequency domain, resulting in:

$$\nabla \times E - i\omega B = 0, \tag{8}$$

and

$$\nabla \times H - J = -J^e, \tag{9}$$

Furthermore, assuming the definition of a grid with connected cells, the finite element method is based on replacing a continuous boundary problem with a discrete one. The region of interest is subdivided into simple elements (triangles, for example) and the Galerkin method is applied to each element.

Computing models can obtain transient data at a sufficient number of frequencies using the fast sine transform, interpolation-based optimized irregular sampling of logarithmic frequency axis, fast Fourier transform (FFT), or logarithmic FFT (FFT-Log). The interpolation-based optimized irregular sampling of logarithmic frequency axis can also min-

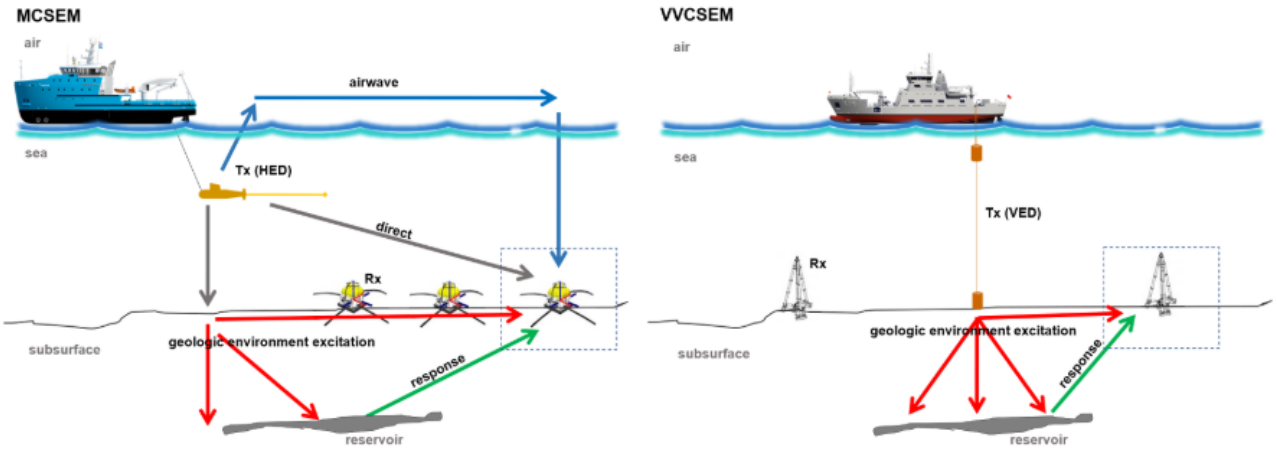

Figure 1: Comparative illustration of the MCSEM and VVCSEM methods. The blue line represents the airwave; the gray, the direct pulse of the Tx; the red, the geologic environment excitation by the Tx; and the green, the response of the interaction between the subsurface and the electric field produced by the source and the reservoir.

imize the frequencies for which full models must be computed for the fast sine transform and logarithmic FFT. Clarification about this can be found in Rijo (2007).

This paper considers the formulations described in Ward and Hohmann (1987) and in Ziolkowski and Slob (2019). As a result, the diffusion equation determines the vertical component of a declining current density and is constant across horizontal borders. The electric diffusion constant D is given by:

$$D = \frac{1}{(\mu\sigma)}, \tag{10}$$

where μ and σ are the magnetic permeability and the electric conductivity, respectively. In a homogeneous half-space, the electric field decays as $Ez(t)\ t^{-2.5}$ at late t. When a layer with reduced electrical conductivity, i.e., a resistive layer, is present, the vertical current density decays more quickly. The scale is simply $d^2 = 2DT$ between the time T, where the modifications are made to the E behaviors $(t)\ t - 2.5$, and the depth d of the HC layer. The most considerable contrast occurs between the times 2 and 10 seconds. The diffusion equation determines the electric current density in a model with variable conductivity layers and such equation can be easily solved to predict the electric field.

The electric dipole moment (at the origin of the coordinate system) is defined as:

$$p = e_x I(t) ds \delta(r), \tag{11}$$

where e_x is the unit vector of the dipole axis, $I(t)$ is the transient pulse, ds is the dipole length and $\delta(r)$ is the Dirac delta function. To solve the problem, Maxwell's equations in terms of the magnetic potential vector A is shown below,

$$\mu\varepsilon\frac{\partial^2 A}{\partial t^2} + \mu\sigma\frac{\partial A}{\partial t} + \nabla \times (\nabla \times A) = 0, \tag{12}$$

Designing and implementing the VVCSEM model

For the three-dimensional models proposed in this manuscript, the COMSOL Multiphysics software was used. The model construction is based on intuitive analogue modeling, but the solution uses numerical methods. COMSOL is a proprietary multiphysics simulation software with several scientific and engineering modules used for building models that are true to reality. The modules expand the functionality of the core platform and are grouped into sections, with electromagnetism being the one of interest in this work.

The finite element methods used for calculating the solution are similar to the finite integration technique (Clemens and Weiland, 2001). However, they are based on variational principles, and they must be formulated only in a domain below the ground surface. Thus, the formulations described in Ward and Hohmann (1987) and in Zhdanov et al. (2006) were considered. Modeling was performed to examine the behavior of the electric field in the time domain in the absence of resistive structures (hydrocarbon reservoirs) with a vertical electric dipole (VED) as a source. Before the simulations and variations of the canonical model (Constable and Weiss, 2006), code validation was performed by comparing the responses of multiphysics VVCSEM with those of the benchmark literature. Holten et al. (2009) and Helwig et al. (2019) are the benchmarks for this paper, as they are responsible for the first and the most recent works published by the creators of the prospecting

methodology and the patent holders, respectively.

The model used in this manuscript was built in several stages. First, the response from the source (switch-on) was calculated in the stationary regime, with the field variables not changing over time but rather as a function of the injected current (5000 A). The stationary study was performed separately, and the response of the source excitation in the half-space was stored for later use.

Next, two other studies were performed in the transient domain: the source response obtained in the previous stationary study is the input signal, thus simulating a switch-off of the source, since in the field survey, information on the electromagnetic field is read by the receivers (Rx) during periods of source (Tx) inactivity.

The first transient study brings the propagation of electromagnetic waves in a geological environment (canonical model) without a reservoir. The second was carried out in a geological environment with a reservoir because, in the analysis of the collected data, the responses in environments where hydrocarbons ($NoHC$) are absent are compared to the response in an environment where hydrocarbons (HC) are present. The analysis domain was defined as a cylinder to optimize memory and computing time in the modeling.

The transmitter (VED) is constructed as a line segment (z-oriented polyline) that has its top (first point) 50 m below sea level and its base (second and last point) in contact with the seafloor. In this model, the water layer is 300 m thick, the source is 250 m long, and the upper electrode is 50 m below sea level.

The receivers were constructed as a polyline on the seafloor. Their points represent the receiver positions at 200 m, 423 m, 894 m, 1891 m and 4000 m. Table 1 elucidates the model geometry by showing the configuration of the transmitter and of the receivers.

After completing the insertion of all necessary geometries for the model, the material definition step begins. The physical characteristics of each layer are specified in this stage. At the top is the air layer, represented by the upper region of the cylinder and with an electrical resistivity of $2x10^{-14}$ $Ohm.m$; it is followed by the sea layer, whose electrical resistivity value is 0.3 $Ohm.m$. In the middle plane of the cylinder, the subsurface (middle or bottom) was specified with a resistivity value of 1 $Ohm.m$. Embedded in the rock/sediment, at an average depth of $700m$, is the top of the hydrocarbon reservoir, with an electrical resistivity of 100 $Ohm.m$. In the reference model used for control, the reservoir layer is hidden, to simulate a control environment, without hydrocarbons.

The mesh construction stage started after the material definition stage had been completed. The mesh is densified in the regions of most interest, mainly around the Tx, the Rx and the reservoir (when present). Figure 2 shows a cross-section of the mesh to enable a better visualization of the details. The mesh was built with variable mesh density; the boundary region (top, bottom and sides) is fine-meshed (minimum element size is 100 m and maximum is 500 m); the air, sea and sediment regions are extra fine-meshed (minimum element size is 10 m and maximum is 100 m); and the reservoir region and the surroundings of the transmitter and receivers are extremely fine-meshed (minimum element size is 5 m and maximum is 10 m). The complete mesh consists of 267,276 domain elements, 43,146 boundary elements, and 1,796 edge elements.

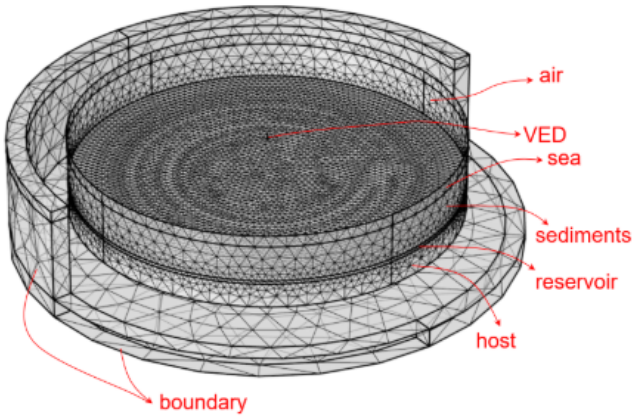

Figure 2: Elements and partitions applied to the >:< 5 model.

In the outermost part of the model, a cylindrical shape with scattering boundary conditions was inserted. These boundary conditions behave as a transparent boundary (shell) for the outgoing waves; therefore, they are not returned in the model. Although the electromagnetic field propagation caused by a VED is shaped like a toroid, the top and bottom were inserted into the Tx with scattering boundary conditions to avoid contamination in the model.

After the study type, mesh and model selection are completed, the simulation is started by computing the source response and then the disconnected source response, as mentioned above. In order to accurately assess the computational time and effort, and to establish a foundation for the hardware selection, a workstation with an Intel Core i7 processor, 64 GB of RAM, and a 2 TB hard drive was utilized. The model simulations had an average runtime of 6 hours. After this step is completed, the results are displayed after the datasets have been set up. In the VVCSEM model, the field response was plotted as plot 3D.

The results can also be displayed in graphical form; the curve is constructed from the logarithmic plot. To analyze the contrast between the background and the anomalous curves, the response of the model ignoring the reservoir layer ($NoHC$) is placed together with the response of the field that has the resistive structure (HC).

Table 1: Model geometry – Configurations of the transmitter and receivers.

Transmitter (Tx)			Receivers (Rx)		
Variable	**Value**	**Description**	**Variable**	**Value**	**Description**
Txx1	0 m	bipole position 1 for x coordinate	Rxx1	200 m	receiver position 1 for x coordinate
Txy1	0 m	bipole position 1 for y coordinate	Rxx2	423 m	receiver position 2 for x coordinate
Txz1	−50 m	bipole position 1 for z coordinate	Rxx3	894 m	receiver position 3 for x coordinate
Txx2	0 m	bipole position 2 for x coordinate	Rxx4	1891 m	receiver position 4 for x coordinate
Txy2	0 m	bipole position 2 for y coordinate	Rxx5	4000 m	receiver position 5 for x coordinate
Txz2	−300 m	bipole position 2 for z coordinate	Rxy	0 m	receiver position for y coordinate
on	1	switch	Rxz	$-h_{\text{sea}}$	receiver position for z coordinate
Amp	5000 A	current strength			

RESULTS

To compare the responses from different perspectives and validate them based on the benchmark literature, a 3D model was built. The first curve shows the wave propagation in an environment without a reservoir and the second one in an environment with a reservoir. In the data analysis, the comparison should be made between the response in a controlled environment with the absence of hydrocarbons (NoHC) and the response in an environment with hydrocarbons (HC). In the comparison, the response of the VVCSEM modeling behaved very similarly to the response reported in the papers of Holten et al. (2009) and Helwig et al. (2019), which are the benchmarks of this work. In the original figure of the benchmark literature (left side of Figure 3), the result expressed in Amplitude in V, in reality, is the field Ez in V/m; the geological environment is called background (Back; continuous orange line); and the environment with the hydrocarbon layer is called resistor (Res; continuous blue line).

The plotted curves show the amplitude of the difference in the interaction between the electromagnetic field and the geological environment with and without the resistive layer. The result of the modeling validation can be seen in Figure 3.

As expected, the result found with the 3D model proved to be very similar to those obtained with the 1D model (benchmark papers). However, somehow, the presence of the layer simulating the three-dimensional hydrocarbon body generated a decaying behavior of minor amplitude at the final times in the curves that describe the field (Res and Back - left; HC and NoHC - right).

After the validation of the 3D response of the VVCSEM, tests were performed to examine the responses of the method in different geological environments. The tests consisted of variations in water layer thickness, reservoir layer thickness, reservoir electrical resistivity, postsalt and presalt reservoir analysis, and Tx tilt ($-10°, +10°, -20° and + 20°$). All tests were performed using the canonical model shown in Figure 2.

Variation in water layer thickness

The layer thickness variation referring to the seawater column was 300 m, 600 m, 1200 m and 2400 m, thus simulating shallow to ultradeep waters, such as those observed in the prospects. The result of the simulations is shown in Figure 4.

Importantly, when there is variation in the seawater column, the size of the Tx (VED) also increases because it is built as a line segment (z-oriented polyline) whose top (first point) is at 50 m below sea level and whose base (second and last point) is in contact with the ocean floor. Thus, the VED has dimensions of 250 m, 550 m, 1150 m and 2350 m for depths of 300 m, 600 m, 1200 and 2400 m, respectively. An offshore survey is a real operational challenge since the source must remain vertically oriented to avoid contaminating other electromagnetic field components. The higher the water depth, the more copper cable is used from the coils present on the transmitter launch platform.

The analysis of the graphs of the VVCSEM responses for the thickness values used in the modeling shows that the larger the water layer, the smaller the contribution of the reservoir layer, even though the increase in sea depth implies an increase in the size of the Tx, but not in the injected current. Notably, the tops of all reservoir structures are at 700 m within the seafloor.

Analyzing quantitatively, the comparison among the four models with varying seawater layer thicknesses shows significant variations at the points of maximum difference. For the 300 m layer, the maximum value occurs at 1.32 seconds, with an electric field magnitude of $8.9 \times 10^{-7} V/m$. In the 600 m model, this point shifts to 1.59 seconds with a magnitude of $2.5 \times 10^{-7} V/m$, representing an 855% increase. For the 1200 m layer, the maximum value is observed at 4.86 seconds with a magnitude of $3.1 \times 10^{-7} V/m$, showing a 1473% relative difference compared to the 300 m model. Lastly, the 2400 m model presents the maximum value at 12.32 seconds with a magnitude of $3.6 \times 10^{-7} V/m$, indicating a 305% variation. These results demonstrate that as the layer thickness increases, the maximum difference occurs later, and

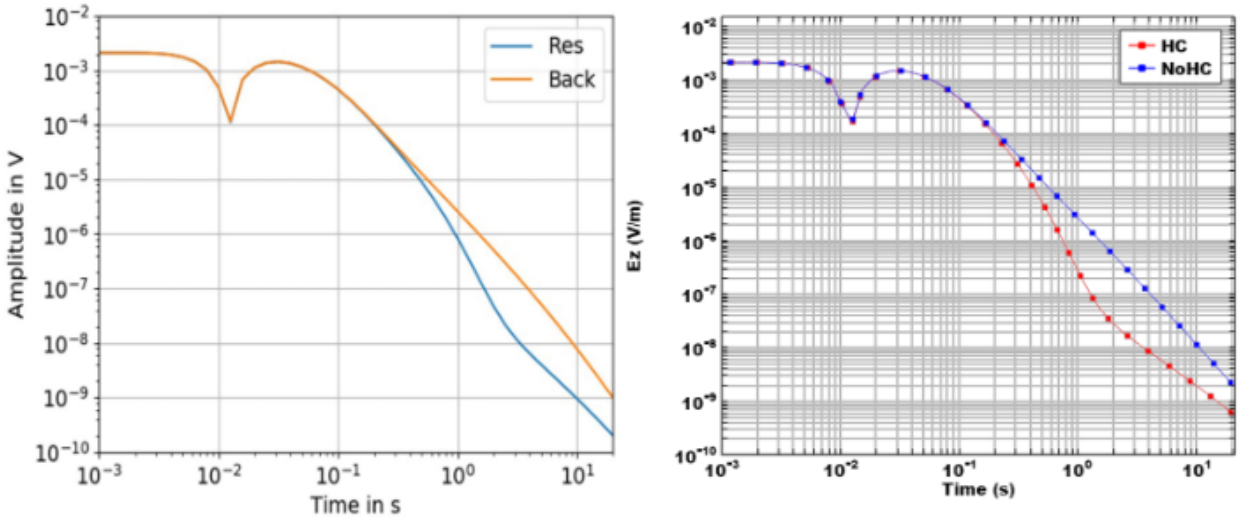

Figure 3: Comparison of the VVCSEM response (1D) from Holten et al. (2009) and Helwig et al. (2019) (left) with the response found with the 3D model in the multiphysics modeler (right), for the canonical model and 200 m offset.

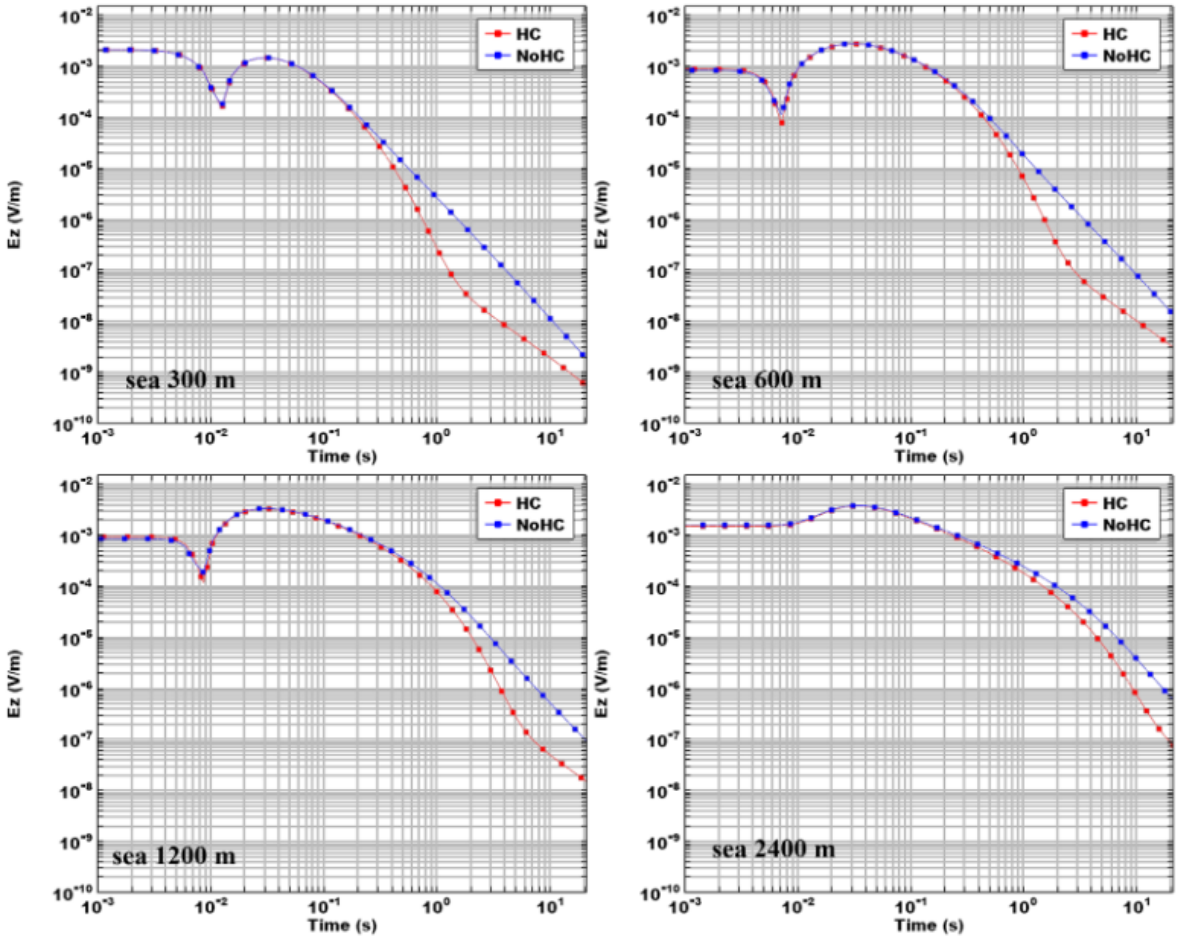

Figure 4: VVCSEM response for the 300 m, 600 m, 1200 m and 2400 m thick water slide (seen from left to right and from top to bottom).

the electric field magnitude also increases, with the largest variations seen between the 1200 m and 300 m models.

Variation in reservoir layer thickness

The variation of the reservoir layer was tested with thickness values of 25 m, 50 m, 100 m and 200 m to verify the sensitivity of the method when using thin to thicker resistors.

The changes in reservoir size did not result in as large a change in the model curves as did the changes in sea depth levels. This probably occurred because the background and the source length did not change. However, the difference between the curves increases in a direct proportion to the increase in the thickness of the HC layer. Figure 5 shows the result of the simulations.

When analyzing the VVCSEM responses generated by the models based on resistor variation, it is clear and expected that the larger the vertical dimension of the resistive layer, the greater the anomaly it causes in the control model since the electromagnetic field decays more quickly in the presence of a structure with low electric conductivity.

Analyzing quantitatively the results, for the 25 m thickness, the maximum value occurs at 1.32 seconds with an electric field magnitude of $3.3 \times 10^{-7} V/m$. In the case of the 50 m layer, the maximum value shifts to 1.09 seconds with a magnitude of $1.7 \times 10^{-7} V/m$. For the 100 m layer, the maximum value is observed at 1.26 seconds, with a magnitude of $8.9 \times 10^{-7} V/m$. Finally, the 200 m layer shows a maximum value at 1.07 seconds with a magnitude of $0.8 \times 10^{-8} V/m$. These results indicate that the method sensitivity is affected by the layer thickness, with variations in both the timing and magnitude of the electric field observed across the different thicknesses.

Variation of electrical resistivity of the reservoir

The variation of the electrical resistivity of the reservoir was performed with values of 100 *Ohm.m*, 90 *Ohm.m*, 80 *Ohm.m* and 10 *Ohm.m*, to verify the effects that occur during the production of an oil field, where the electrical resistivity of the reservoir decreases as petroleum (oil and gas) is surveyed and where salty water is injected to boost pressure during production.

The variations in the electrical resistivity of the reservoir caused significant changes in the model curves, and the disparity between the responses diminished proportionately to the drop in the electrical resistivity of the HC layer. Figure 6 shows the result of the simulations.

We can easily determine the VVCSEM responses generated by the models with variation in the electrical resistivity of the resistor. As expected, the higher and the longer-lasting field production is, the lower the anomaly caused by variation in electrical resistivity in the control model. For example, the analysis of the curves with 100 *Ohm.m* and 90 *Ohm.m* shows that there is a subtle difference; when seen separately, these curves are indistinguishable, as the electrical resistivity values that generated the anomaly are not known; however, the finding suggests that the method is efficient to monitor reservoirs as it shows a history of signs over a time-lapse.

Analyzing quantitatively, the variation of the electrical resistivity of the reservoir was conducted using values of 100 *Ohm.m*, 90 *Ohm.m*, 80 *Ohm.m* and 10 *Ohm.m* to investigate the effects that occur during oil field production. As petroleum (oil and gas) is extracted and salty water is injected to enhance pressure during production, the electrical resistivity of the reservoir decreases. For the 100 *Ohm.m* layer, the maximum value occurs at 1.26 seconds with an electric field magnitude of $8.9 \times 10^{-7} V/m$. The 90 *Ohm.m* layer, in comparison, shows a maximum value at 1.32 seconds, but with a slightly higher magnitude of $9.9 \times 10^{-7} V/m$. For the 80 *Ohm.m* layer, the maximum value remains at 1.26 seconds with a magnitude of $6.1 \times 10^{-7} V/m$. Finally, the 10 *Ohm.m* layer shows a maximum value at 0.75 seconds with a magnitude of $6.9 \times 10^{-6} V/m$. These results illustrate that as resistivity decreases, the electric field magnitude tends to increase, reflecting the changes in reservoir saturation and connectivity during the production process.

Variation in the postsalt reservoir

The analysis of variation in the response of the postsalt reservoir was performed by inserting a layer with electrical resistivity values of 500 *Ohm.m*, 1000 *Ohm.m*, 1500 *Ohm.m* and 2000 *Ohm.m* just below the HC layer, aiming to verify the sensitivity of the method in geological environments with reservoirs adjacent to saline structures (domes, pillows, intrusions/diphones and other salt formations). . The insertion of the resistor layer underneath the layer simulating the hydrocarbon promoted a fast decay of the electromagnetic field and also the hydrocarbon anomaly mixed with the salt anomaly. The response collected by the Rx suffered so much interference that a new scale (axis) was used to enable the visualization of the data. The result of the simulations is shown in Figure 7.

A comparison of the VVCSEM responses generated by the postsalt models shows that the anomaly they produced in the control model is quite discrepant. The highly resistive salt layer masks the response of the reservoir, and the electromagnetic method has shown some inaccuracy in the data, similarly to what happens with an elongated blade or salt canopy. A second disambiguating method will be ideally used in the presence of the nonpoint salt and very close to the target of interest.

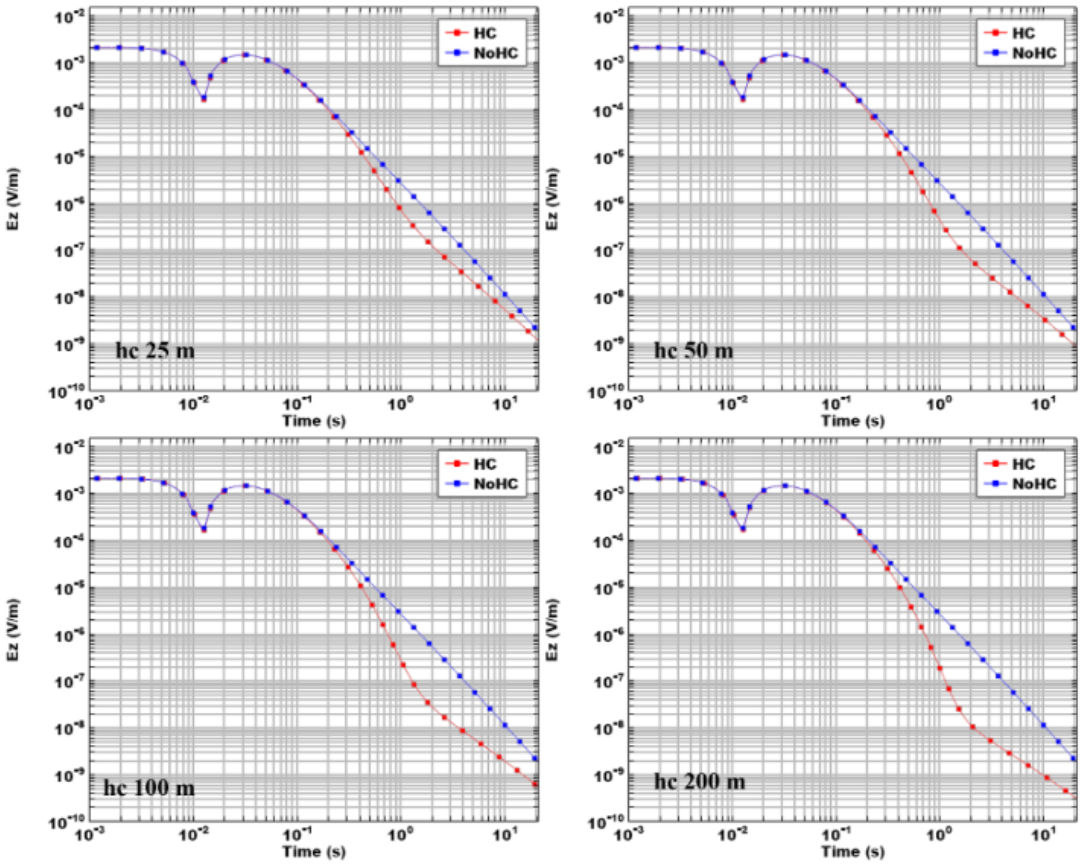

Figure 5: VVCSEM response for reservoir thickness values of 25 m, 50 m, 100 m and 200 m (seen from left to right and from top to bottom).

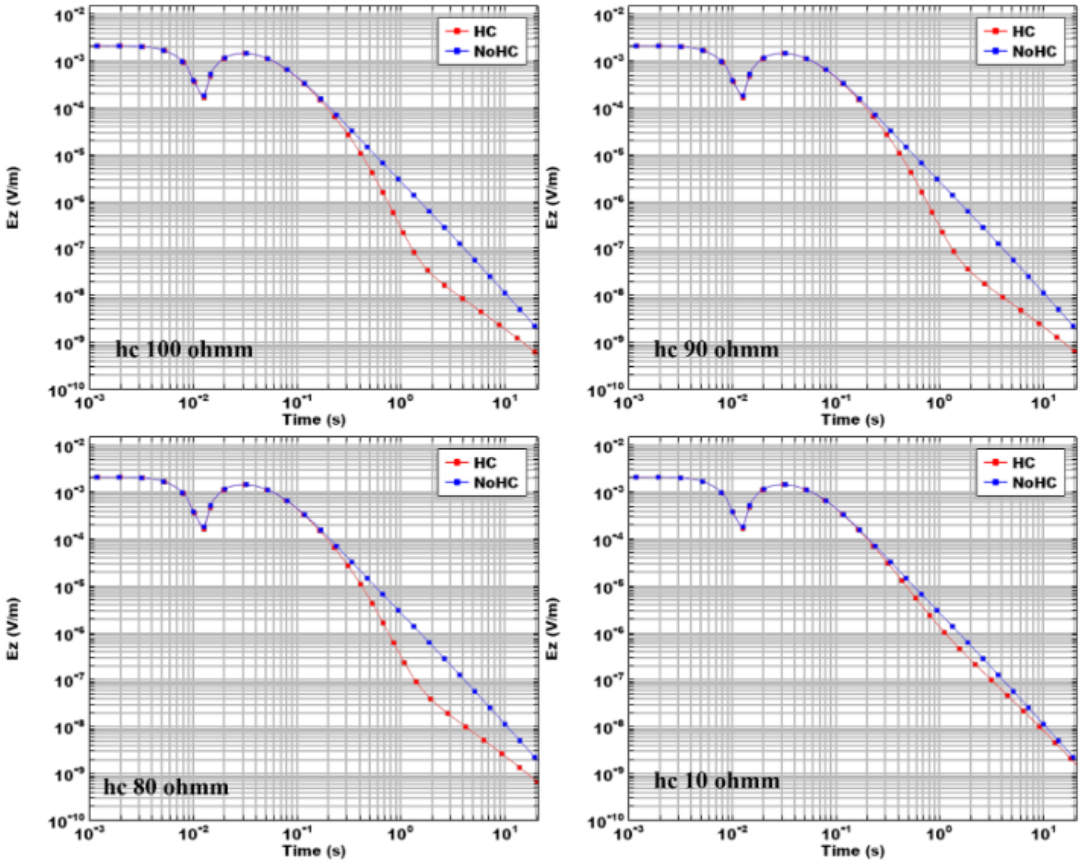

Figure 6: VVCSEM response for variation of electrical resistivity of the reservoir with values of 100 Ohm.m, 90 Ohm.m, 80 Ohm.m and 10 Ohm.m (seen from left to right and from top to bottom).

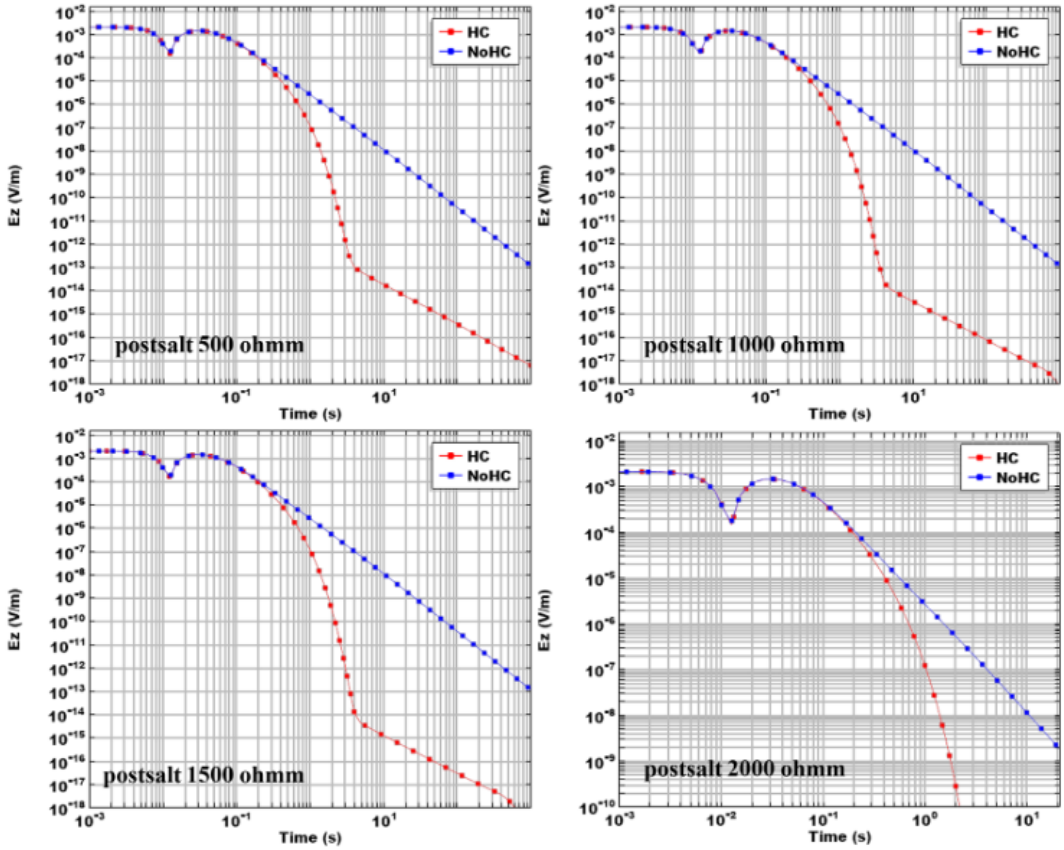

Figure 7: VVCSEM response for variation in the postsalt reservoir for electrical resistivity values of 500 Ohm.m, 1000 Ohm.m, 1500 Ohm.m and 2000 Ohm.m (seen from left to right and from top to bottom).

Analyzing quantitatively, the analysis of variation in the response of the postsalt reservoir was performed by inserting a layer with electrical resistivity values of 500 $Ohm.m$, 1000 $Ohm.m$, 1500 $Ohm.m$ and 2000 $Ohm.m$ just below the hydrocarbon (HC) layer. This analysis aimed to verify the sensitivity of the method in geological environments with reservoirs adjacent to saline structures. For the 500 $Ohm.m$ layer, the maximum value occurs at 3.35 seconds with an electric field magnitude of $3.6 \times 10^{-13} V/m$. In the case of the 1000 $Ohm.m$ layer, the maximum value shifts to 3.58 seconds with a magnitude of $2.3 \times 10^{-14} V/m$. For the 1500 $Ohm.m$ layer, the maximum value is observed at 4.03 seconds with a magnitude of $4.6 \times 10^{-15} V/m$. Finally, the 2000 $Ohm.m$ layer shows a maximum value at 5.85 seconds with a magnitude of $1.1 \times 10^{-16} V/m$. These results indicate that as the resistivity increases, both the timing and the magnitude of the electric field response exhibit significant changes, providing insight into the interaction between hydrocarbon reservoirs and adjacent saline structures.

Variation in the presalt reservoir

A presalt reservoir simulation was performed by inserting a layer with electrical resistivity values of 500 $Ohm.m$, 1000 $Ohm.m$, 1500 $Ohm.m$ and 2000 Ohm.m just above the HC layer. Similarly to the postsalt modeling, the objective of this simulation was to verify the sensitivity of the method in geological environments with reservoirs adjacent to saline structures.

The anomaly generated by the degradation of the electromagnetic field caused by the installation of the resistive layer above the hydrocarbon-simulating layer had no significant influence on the recorded data. Thus, the presalt anomaly was not much different from the anomaly caused by the variation in the electrical resistivity of the reservoir itself. Figure 8 shows the result of the simulations.

When checking the VVCSEM responses generated by the presalt models, it is clear that the method, in this configuration, could hardly distinguish the salt layer, even though it is highly resistive. The plot of the electromagnetic field response for the model with a 200 $Ohm.m$ reservoir (Variation of the electrical resistivity of the reservoir - Figure 6) resembles the response obtained with a 100 $Ohm.m$ reservoir and a 500 $Ohm.m$ saline layer above.

Analyzing quantitatively, a presalt reservoir simulation was performed by inserting a layer with electrical resistivity values of 500 $Ohm.m$, 1000 $Ohm.m$, 1500 $Ohm.m$ and 2000 $Ohm.m$ just above the hydrocarbon (HC) layer. For the 500 $Ohm.m$ layer, the maximum value occurs at 0.91 seconds with an electric field magnitude of $2.6 \times 10^{-7} V/m$. In the case of the 1000 $Ohm.m$ layer, the maximum value shifts

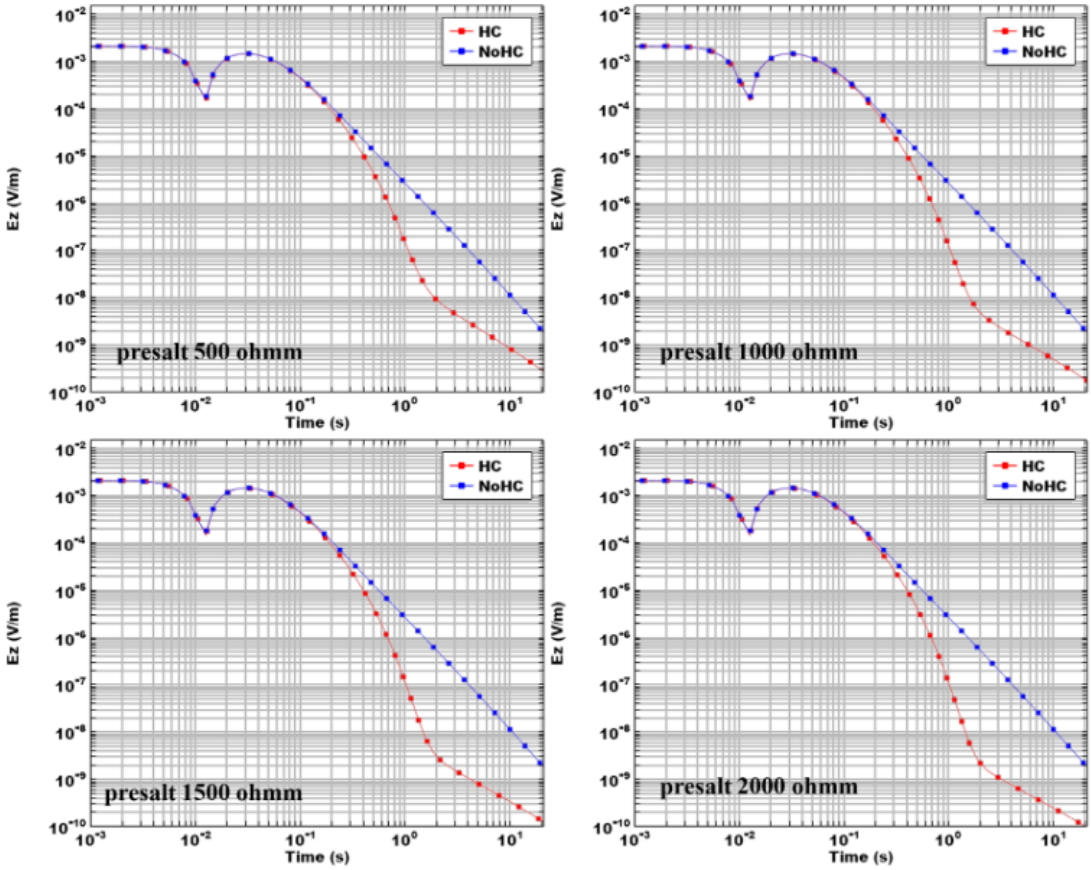

Figure 8: VVCSEM response for variation in the presalt reservoir for electrical resistivity values of 500 Ohm.m, 1000 Ohm.m, 1500 Ohm.m and 2000 Ohm.m (seen from left to right and from top to bottom).

to 1.09 seconds with a magnitude of $7.7 \times 10^{-8} V/m$. For the 1500 $Ohm.m$ layer, the maximum value is observed at 1.32 seconds with a magnitude of $2.0 \times 10^{-8} V/m$. Finally, the 2000 $Ohm.m$ layer shows a maximum value at 1.59 seconds with a magnitude of $1.8 \times 10^{-8} V/m$. These results indicate a notable decrease in the electric field magnitude as resistivity increases, suggesting complex interactions in the presalt reservoir environment.

Variation of Tx tilt

The variation of Tx tilt was tested with tilts of $-10°, +10°, -20° and + 20°$ to analyze the variations in the responses of the VVCSEM in environments with very rough bathymetry, causing misalignment of the verticality of the transmitter. Even when these tilts are small, they are undesirable and should be avoided; however, knowledge of their effects on the acquired data helps with quality control and interpreting the findings. The simulation results are shown in Figure 9.

The analysis of the VVCSEM responses for different tilts of the Tx shows that they lead to changes in large-field measurements. When the Tx stimulates the geological environment in misalignment with the vertical or horizontal orientation, several components of the electromagnetic field mix, and a disagreement occurs between the transverse magnetic (TM: H_y, E_x and E_z components) and transverse electric (TE: E_y, H_x and H_z components) propagation modes. Thus, with the Tx tilt effect, the Rx picks up a resultant contaminated field.

The most significant changes in the simulation responses occurred in the shift peaks, especially at the $+20°$ tilt. The responses between the $-10°$ and $-20°$ tilts are similar, but the responses between$+10°$ and$+20°$ are very distinct from each other and from the other responses. Notably, during the VVCSEM acquisitions, the tilt should be a maximum of $+1°$, equivalent to a Tx length deviation of 3 m, owing to the displacement of the upper pole in relation to the lower pole. The oversized values used here are only for better visualization of the tilt effects on the acquired data.

Analyzing quantitatively, the variation of Tx tilt was tested with tilts of $-10°, +10°, -20°$ and $+20°$ to analyze the variations in the responses of the VVCSEM in environments with very rough bathymetry, causing misalignment of the transmitter verticality. For the $-10°$ tilt, the maximum value occurs at 0.91 seconds with an electric field magnitude of $4.2 \times 10^{-7} V/m$. The $+10°$ tilt shows a maximum value at 1.32 seconds with a magnitude of $4.5 \times 10^{-8} V/m$. For the $-20°$ tilt, the maximum value is observed at 0.91 seconds with a magnitude of $4.1 \times 10^{-7} V/m$. Lastly,

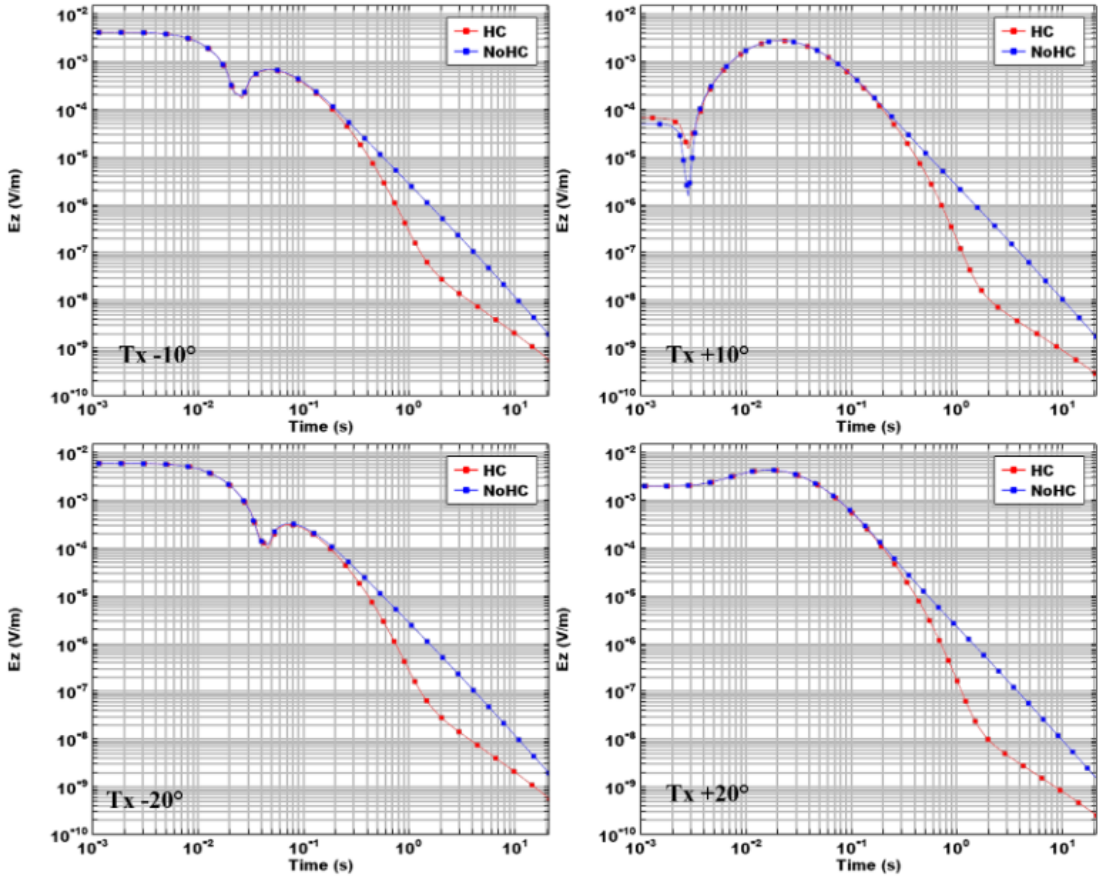

Figure 9: The VVCSEM response for variation of Tx performed with tilts of $-10°, +10°, -20°$ and $+20°$ (seen from left to right and from top to bottom)

the $+20°$ tilt has a maximum value at 1.05 seconds with a magnitude of $4.7 \times 10^{-8} V/m$. These results indicate that the tilt variations impact the electric field responses, suggesting that tilts significantly affect the measurement accuracy in environments with challenging bathymetric conditions.

Future studies intend to develop more complex models until they can implement the VVCSEM response directly in a realistic geological model, such as Marlim R3D (Carvalho and Menezes, 2017; Correa and Menezes, 2019). The geological model represented a Brazilian turbidite reservoir with 6 (six) stratigraphic horizons and was obtained from the analysis of seismic profiles (2D and 3D) arranged in parallel and transversally in the area of interest, which were correlated with well-logging data present in the region.

CONCLUSIONS

The VVCSEM method has proven competent in identifying resistive anomalies originating from hydrocarbon reservoirs, even in different models. This efficiency can be observed in the results published in the literature and by the model presented in this paper. However, there were also ambiguous situations, but *a priori* information, based on knowledge of the local geology, combined with other geophysical methodologies, helped to reduce the occurrence of these situations.

Numerical modeling using the multiphysics modeler provided good results for the proposed models for the environment (variation in geometry), production and monitoring (resistivity), and the instrumental (tilt) tests.

ACKNOWLEDGMENTS

The authors are thankful to the Geophysics Faculty/UFPA and CPGf/UFPA, for the infrastructure, to Fundação Amparo e Desenvolvimento da Pesquisa (FADESP - foundation for support and development of research) and also to Petrobras, for providing the academic license for the multiphysics modeler. The first author thanks the Coordination for the Improvement of Higher Education Personnel (CAPES) and the National Council for Scientific and Technological Development (CNPq) for providing the scholarship.

REFERENCES

Barsukov, P., E. B. Fainberg, and B. Singer, 2007, A method for hydrocarbon reservoir mapping and apparatus for use when performing the method: https://patentscope.wipo.int/search/en/WO20070

53025. (PCT/NO2006/000372).
Barsukov, P. O., E. B. Fainberg, and B. Singer, 2008, A method of mapping hydrocarbon reservoirs in shallow waters and also an apparatus for use when practising the method: https://patentscope.wipo.int/search/en/WO2008066389. (PCT/NO2007/000416).
Carvalho, B. R., and P. T. Menezes, 2017, Marlim R3D: a realistic model for CSEM simulations – phase I: model building: Brazilian Journal of Geology, **47**, 633–644, doi: 10.1590/2317-4889201720170088.
Clemens, M., and T. Weiland, 2001, Discrete electromagnetism with the Finite Integration Technique: Journal of Electromagnetic Waves and Applications, **15**, 79–80, doi: 10.1163/156939301X00661.
Constable, S., and C. J. Weiss, 2006, Mapping thin resistors and hydrocarbons with marine EM methods: insights from 1D modeling: Geophysics, **71**, G43–G51, doi: 10.1190/1.2187748.
Correa, J. L., and P. T. Menezes, 2019, Marlim R3D: a realistic model for controlled-source electromagnetic simulations – phase 2: the controlled-source electromagnetic data set: Geophysics, **84**, E293–E299, doi: 10.1190/geo2018-0452.1.
Flekkøy, E. G., T. Holten, and D. Veiberg, 2009, Vertical electric time-domain responses from a vertical current source for offshore hydrocarbon exploration: Presented at the Proceedings of the 71st EAGE Conference and Exhibition Incorporating SPE EUROPEC 2009, European Association of Geoscientists & Engineers. doi: 10.3997/2214-4609.201400504.
Frafjord, O., T. Holten, A. M. El Kaffas, J. M. Borven, and S. L. Helwig, 2014, Minimizing the noise contribution in vertical electric field measurements: Presented at the Proceedings of the 76th EAGE Conference and Exhibition 2014, EAGE Publications BV. doi: 10.3997/2214-4609.20141247.
Helwig, S. L., W. Wood, and B. Gloux, 2019, Vertical-vertical controlled-source electromagnetic instrumentation and acquisition: Geophysical Prospecting, **67**, 1582–1594, doi: 10.1111/1365-2478.12771.
Helwig, S. L., W. Wood, B. Gloux, and T. Holten, 2016, A new generation of vertical CSEM receiver: Presented at the Proceedings of the 78th EAGE Conference and Exhibition 2016, European Association of Geoscientists & Engineers. doi: 10.3997/2214-4609.201600561.
Holten, T., E. G. Flekkøy, B. Singer, E. M. Blixt, A. Hanssen, and K. J. Måløy, 2009, Vertical source vertical receiver, electromagnetic technique for offshore hydrocarbon exploration: First Break, **27**, doi: 10.3997/1365-2397.27.1299.28934.
Kjerstad, J., 2010, Device for a vertical electromagnetic field component receiver. (PCT/NO2009/000352).
Rijo, L., 2007, Electrical geophysics 2-D & 3-D earth modeling. Lecture Notes: Graduate Program in Geophysics – UFPA.
Sainson, S., 2017, Electromagnetic seabed logging: Springer International Publishing.
Souza, D. M., M. W. C. Silva, and V. C. T. Souza, 2022, VVCSEM repository.
Ward, S. H., and G. W. Hohmann, 1987, Electromagnetic theory for geophysical applications, *in* Electromagnetic methods in applied geophysics – theory: Society of Exploration Geophysicists, volume **3** *of* SEG Investigations in Geophysics, 130–311. doi: 10.1190/1.9781560802631.ch4.
Zhdanov, M. S., S. K. Lee, and K. Yoshioka, 2006, Integral equation method for 3D modeling of electromagnetic fields in complex structures with inhomogeneous background conductivity: Geophysics, **71**, G333–G345, doi: 10.1190/1.2358403.
Ziolkowski, A., and E. Slob, 2019, Introduction to controlled-source electromagnetic methods: University Printing House.

Souza, D.M.: Programming of the physics interface and the models in the multiphysics modeler, development of the geological model to isolate the reservoir, writing – original draft preparation; **Silva, M.W.C.:** Suggestion of the oilfield case for VVCSEM analysis. writing – review & edition; **Tocantins, V.C.:** Supervision of the programming of the interface and the VVCSEM examples.

Received on November 29, 2023 / Accepted on November 05, 2024